Communications

Mechanical Deformation of Dendrites by Fluid Flow

J. PILLING and A. HELLAWELL

It is generally accepted that liquid agitation during alloy solidification assists in crystal multiplication, as in dendrite fragmentation and the detachment of side arms in the mushy region of a casting. Even without deliberate stirring by electromagnetic or mechanical means, there is often vigorous interdendritic fluid flow promoted by natural thermosolutal convection. Interdendritic fluid flow rates in metals might be as high as 10 mm s^{-1}.[1] It is the purpose of this article to examine whether such fluid flow can cause mechanical deformation of dendrites, sufficient to cause side arms to bend or break. Metals are so ductile at their melting points that applied forces could only be expected to cause bending, as opposed to fracture, although there are no reports of which we are aware of dendritic arms being mechanically bent in this way. The following estimates demonstrate why even bending is not to be expected.

Figure 1 is an example of an ammonium chloride dendrite growing into an aqueous solution between two glass slides, under steady state conditions, with no fluid flow. In this "alloy," there is a very small solid fraction and wide primary spacing—this is a fairly extreme example and in a majority of "real" cases the dendrite side arms would be shorter and thicker. As is usual, there is considerable ripening of side arms and most of them develop narrow necks at the roots where they attach to the primary dendrite stem. There is no significant side arm detachment unless the growth rate falls and/or the temperature is raised.[2,3]

In this analysis, we shall estimate the stress at the root of a secondary dendrite arm of aluminum arising from the action of a flow of molten metal past the dendrite arm. The schematic geometry of the dendrite is shown in Figure 2. Both the root and main sections of the dendrite are assumed to be cylindrical with diameters d_r and d and lengths L_r and L, respectively. In typical castings, the main diameter would vary from 10 to 25 μm, while the root diameters might be between 5 and 10 μm. With flow velocities up to 10^{-2} m s^{-1} and viscosity of 3.12×10^{-3} kg m^{-1} s^{-1},[4] the upper bound for the Reynolds number would be

$$\mathrm{Re} = \frac{v \cdot \rho \cdot d}{\eta} = \frac{10^{-2} \cdot 2.7 \times 10^{3} \cdot 25 \times 10^{-6}}{3.2 \times 10^{-3}} = 0.22 \quad [1]$$

so that it is reasonable to assume streamline flow and that there would be negligible turbulence on the downstream side of the dendrite arm. The shear stress acting along the tangential direction on the surface of the cylinder, $\tau_{r\theta}$, due to drag and the hydrostatic pressure $P_{r\theta}$ would be[5]

$$\tau_{r\theta} = \frac{3\eta v}{2r} \sin(\theta)$$
$$P_{r\theta} = \frac{3\eta v}{2r} \cos(\theta) \quad [2]$$

The force acting in the y direction (parallel to the flow) would be

$$F_y = \tau_{r\theta} \cdot \sin(\theta) + P_{r\theta} \cdot \cos(\theta)$$
$$F_y = \frac{3\eta v}{2r} \quad [3]$$

The total force, F_T, acting on the dendrite arm in the direction of fluid flow can be obtained by integrating F_y over the surface area, A, of the dendrite, *i.e.*,

$$F = 2 \int_0^L \int_0^\pi F_y \, r \, d\theta \, dx \quad [4]$$

since

$$A = 2 \int_0^L \int_0^\pi r \theta \, d\theta \, dx = 2 \pi r L \quad [5]$$

Thus, approximately, the force per unit length, F, would be

$$F = 3 \pi \eta v \quad [6]$$

which is independent of the radius and would be $\sim 3 \times 10^{-4}$ N m^{-1} in the current example.

The skin stress in the dendrite arm, as a function of position along the dendrite arm, can be estimated from

$$\sigma(x) = \frac{-M(x) \cdot r(x)}{I(r(x))} \quad [7]$$

where M is the bending moment, I the moment of inertia of the section, and r the radius, all of which vary with distance from the end of the dendrite arm.

$$M(x) = \frac{-Fx^2}{2} \quad [8]$$

$$I(r(x)) = \frac{\pi (r(x))^4}{4} \quad [9]$$

An analysis of Eq. [7] shows that the tensile stress increases parabolically with distance from the far end of the dendrite arm until the root is reached, with the maximum tensile stress being ~ 0.01 of the estimated yield strength of the material at the melting point (Appendix). At the root, the tensile stress jumps abruptly as the cross section decreases. The maximum tensile stress at the root of the dendrite arm is plotted in Figure 3, normalized with respect to the estimated yield strength of the metal for several root radii as a function of dendrite arm length.

It is apparent from Figure 3 that even with extreme dimensions (*i.e.*, large ratio L/r), the stress in a dendrite arm will lie below that for plastic flow and, in general, that response to interdendritic fluid flow will only be elastic. Estimates of the bending deflection using the second moment area theorem give dendrite tip deflections, δ, of $0.01\ \mu\mathrm{m} < \delta < 0.5\ \mu\mathrm{m}$ for a root radius of 5 μm and $200\ \mu\mathrm{m} < L < 500\ \mu\mathrm{m}$; *i.e.*, any elastic deflection of the dendrite

J. PILLING, Associate Professor, and A. HELLAWELL, Professor, are with the Department of Metallurgy and Materials Engineering, Michigan Technological University, Houghton, MI 49931.

Manuscript submitted March 13, 1995.

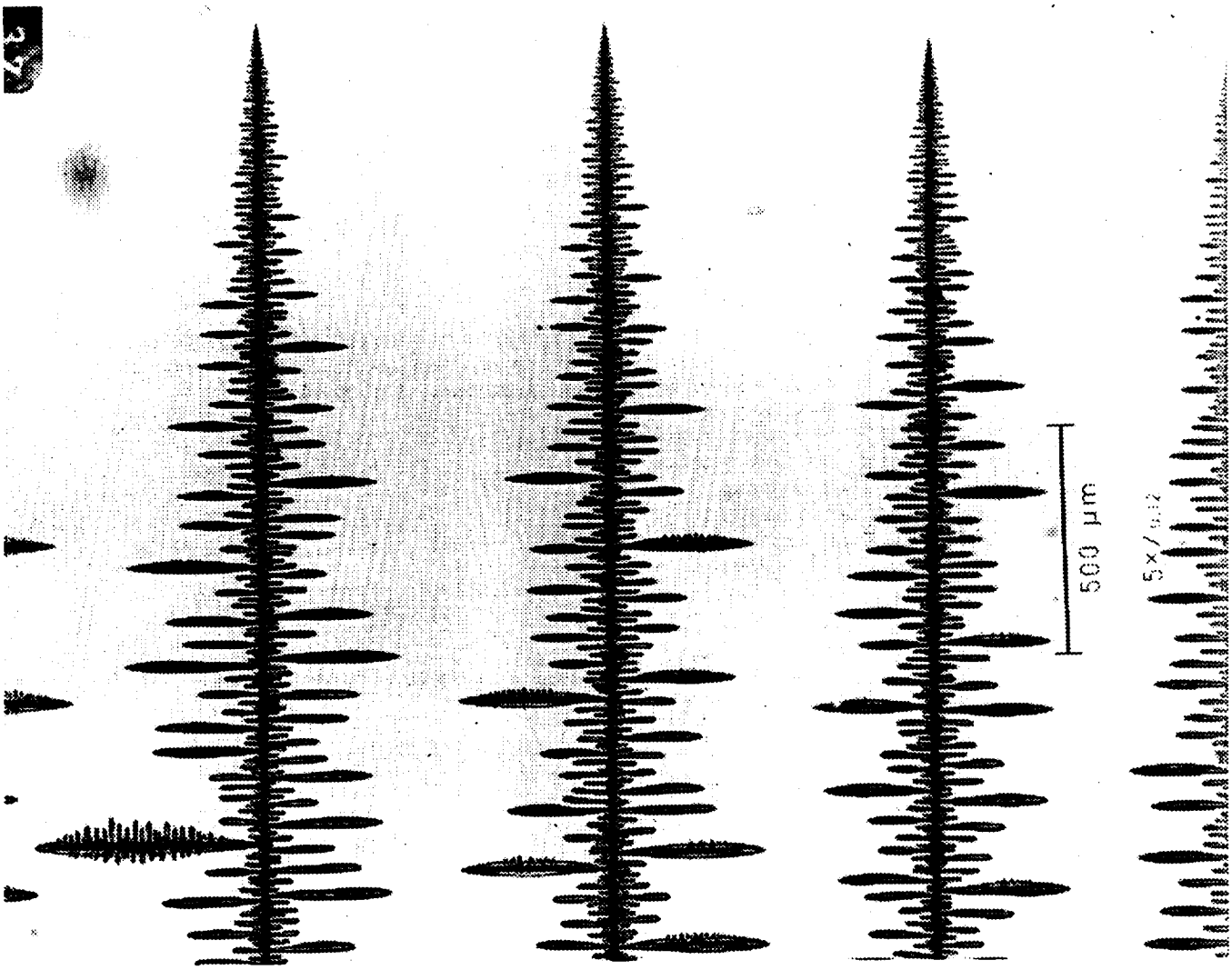

Fig. 1—NH_4Cl dendrites growing from aqueous solution under steady state conditions on a gradient stage: growth rate 28 μm s^{-1} and temperature gradient 6.5 K mm^{-1}. Minimum secondary arm necks are of diameters 5 to 10 μm.

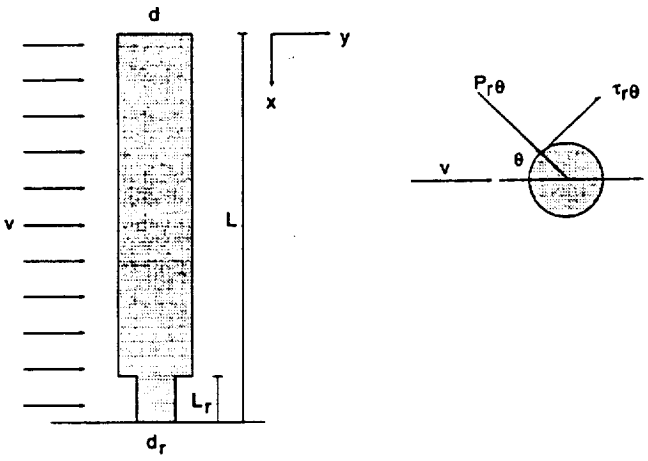

Fig. 2—Geometry of dendrite arm, length L with root length L_r, acted upon by a fluid flowing with a velocity v.

arm will not, at least visually, be apparent. Thus, dendrite fragmentation by mechanical deformation is improbable and other factors cause detachment of side arms.

We note also that these calculations were made with a lower estimate for the elastic modulus and yield stress at the melting point and that an interdendritic flow rate of 10^{-2} m s^{-1} is probably an upper limit, so that the input has been weighted toward the possibility of plastic deformation.

Some brief comments on related matters are in order.

(1) *Secondary Arm Necking*: During cooling in the dendritic array, dendrites are ripening and coarsening, but they are also growing, *i.e.*, the average solid fraction is increasing. Consequently, especially during the earlier stages of ripening, solute rejection occurs simultaneously, radially, from primary and secondary arms, with reinforcement of solute at the junctions or nodes. This locally high solute accumulation causes the initial necks to develop at the roots of side arms, where two curvatures develop with radii r_1 and r_2 of opposite sign (Figures 1 and 4). Therefore, the depression of the freezing point from curvature is actually very small:

$$\Delta T_r = \frac{\sigma_{SL}}{\Delta S}\left(\frac{1}{r_1} - \frac{1}{r_2}\right) \to 0 \qquad [10]$$

where σ_{SL} is the solid liquid surface energy and ΔS is the

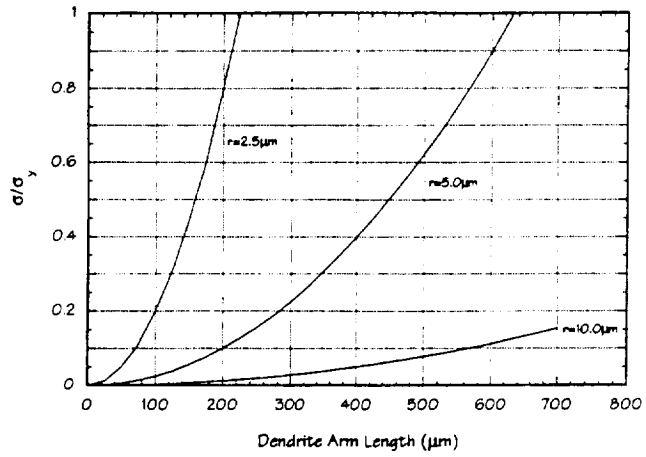

Fig. 3—Calculated stress levels, σ, in dendrite arms with an assumed flow rate of 10^{-2} m s^{-1}, using data for aluminum, expressed as a fraction of the yield stress, σ_y, *vs* arm length for three radii.

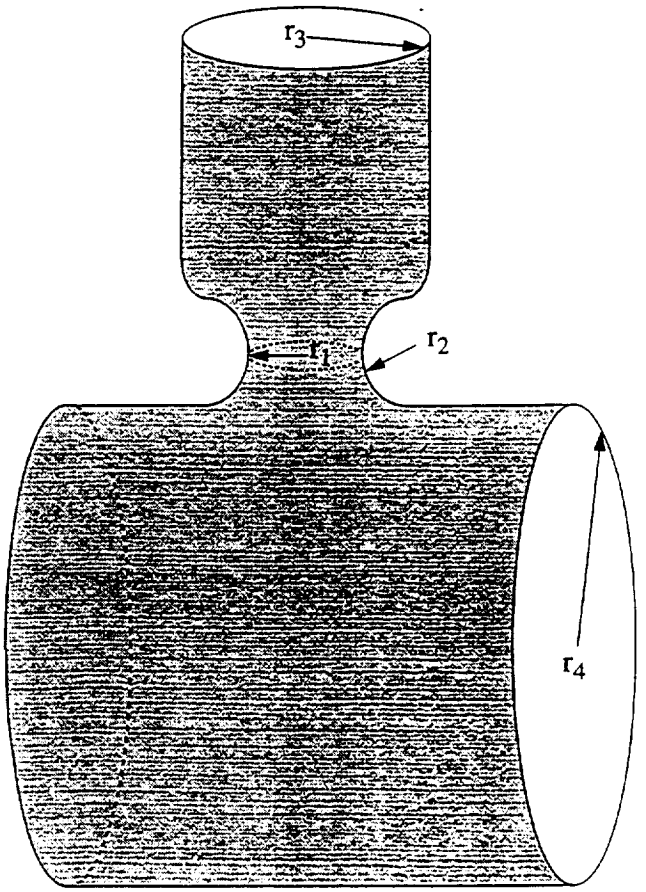

Fig. 4—Schematic representation of various radii of curvature at a side arm root and within a dendritic array, r_1, r_2, *etc.*

entropy of fusion. For this reason, the curvature balance allows these necked roots to persist in equilibrium with the array for long times, unless either the ambient temperature or the ambient interdendritic solute concentration rises. Lower observed values of r_1 and r_2 are about 2.5 μm (Figure 1). Taking data for aluminum,[6] the Gibbs–Thompson coefficient $\Gamma = \sigma_{SL}/\Delta S \approx 10^{-7}$ mK, and this gives curvature undercoolings of ± 0.04 K around such regions, compared with values for the broader primary and secondary cylinders, r_3, r_4, *etc.*, which are an order of magnitude smaller. If r_1 and/or r_2 decrease further, the balance between them and the rest of the assembly obviously becomes very delicate and any slight perturbation causes almost instantaneous detachment. Mechanical deformation during the brief interval of separation would not be a significant factor affecting the *rate* at which this occurred.

(2) *Melting–Side Arm Detachment*: Entrainment of bulk liquid behind a dendritic growth front, whether promoted by forced stirring or convective recirculation, introduces warmer liquid into the mushy array, and, at first impression, this might be thought to accelerate side arm detachment by melting. However, it must be remembered that this liquid is always less concentrated (*i.e.*, is solvent rich), so that as it is drawn or driven into the mushy region and cooled, solvent is deposited and growth accelerated, rather than the reverse. Inasmuch as this entrainment of the bulk liquid must involve growth, it does not seem to be a very probable cause of side arm detachment.

What most clearly does promote the melting off of side arms, more effectively than anything else, is deceleration of the dendritic growth front.[2] In the columnar region of a casting, the growth front is always decelerating, approximately parabolically, and the temperature gradient is falling. Under steady state conditions, a preferred stable primary spacing and tip curvature prevail (*e.g.*, Reference 7), but with deceleration, although the tip curvature changes immediately with velocity ($r^2V \approx$ constant), the primary spacings adjust more slowly (*e.g.*, References 2 and 8) and are always smaller at a given rate than the steady state, stable solution.[9] Consequently, the conditions at the actual growth front are always incompatible with those behind the front, where growth took place more rapidly. This transient hysteresis effect continuously raises the local solute concentration (and temperature) within the array and thus promotes melting and detachment which are not evident under steady state conditions.

It may be concluded that interdendritic fluid flow does not contribute directly to crystal multiplication by causing dendrite fragmentation, but instead aids in the transport of those dendrite fragments which have already formed by another mechanism. This may seem to be a minor point from a practical standpoint, but it is surely important in understanding what is actually happening.

APPENDIX

The yield strength at the melting point can be estimated following the method of Frost and Ashby:[10]

$$\sigma_y(T) = 10^{-3} \cdot E(T)$$

$$E(T) = E_{300}\left(1 + B \cdot \left(\frac{T - 300}{T_m}\right)\right)$$

Where $E(T)$ is the elastic modulus at an absolute temperature T, E_{300} is the modulus at 300 K, and T_m is the absolute melting temperature. Taking E_{300} as 67 GPA and B as

-1.33, we obtain $\sigma_y(T_m) = 6.5$ MPa. Previous experiments to determine the creep/superplastic behavior of aluminum base alloys at temperatures up to 540 °C have shown that these stresses would correspond to a strain rate of $\sim 10^{-3}$ s^{-1}.[11] Consequently, we have reduced the anticipated yield stress by an order of magnitude to 0.6 MPa, where strain rates of $\approx 5 \times 10^{-5}$ s^{-1} would be expected and hence more in keeping with a concept of (normal) elastic behavior within the time scales experienced during solidification.

Figures 1 and 4 are from unpublished work by G.C. Hansen (MTU). This work is part of a research program concerned with intrinsic nucleation and the grain structure of castings, supported by the National Science Foundation, Division of Materials Research, Metallurgy Program, Grant No. DMR 92-06783, and the National Aeronautics and Space Administration, Microgravity Program, through NASA–Lewis Research Center, Grant No. NAG-3-1462.

REFERENCES

1. A. Hellawell, J.R. Sarazinn, and R.S. Steube: *Phil Trans. R. Soc. London*, 1993, vol. A345, pp. 507-44.
2. K.A. Jackson, J.D. Hunt, D.R. Uhlmann, and T.P. Seward: *Trans. TMS-AIME*, 1966, vol. 236, pp. 149-60, Figure 7.
3. T. Sato, W. Kurz, and K. Ikawa: *Trans. Jpn. Inst. Met.*, 1987, vol. 28, pp. 1012-21.
4. Y. Waseda and K. Suzuki: *Phys. Status Solidi B*, 1973, vol. 57, pp. 351-67.
5. D.R. Gaskell: *An Introduction to Transport Phenomena in Materials Engineering*, MacMillan, New York, NY, 1992, pp. 125-30 and 163-66.
6. W. Kurz and D.J. Fisher: *Fundamentals of Solidification*, Trans Tech Publications, Aedermannsdorf, Switzerland, 1984, Appendix 12.
7. J.D. Hunt and S.Z. Lu: *TMS Fall Meeting*, Rosemont, IL, 1994, in press.
8. R.A. Pratt and R.N. Grugel: *Mater. Characterization*, 1993, vol. 31, pp. 225-31.
9. A. Hellawell: in *Modelling of Casting, Welding and Advanced Solidification Processes, VII*, Keynote Address, in press.
10. H.J. Frost and M.F. Ashby: *Deformation Mechanism Maps*, Pergamon Press, Oxford, United Kingdom, 1982, p. 21.
11. J. Pilling and N. Ridley: *Acta Metall.*, 1986, vol. 34, pp. 669-79.

Modeling of Dynamic Material Behavior: A Critical Evaluation of the Dissipator Power Co-content Approach

F. MONTHEILLET, J.J. JONAS, and K.W. NEALE

Several articles have been published recently in which the high-temperature forming of metals has been analyzed in terms of the *dissipator content* G and the *dissipator co-content* J.[1-8] Because of the interest elicited by this approach, which involves predicting the temperature and strain rate ranges over which optimum workability is expected to be attained, it seems opportune to re-examine the foundations of this analysis and to consider how it can be given a physical interpretation.

We begin by recalling the conventional definitions[9] of G and J:

$$G(\dot{\boldsymbol{\varepsilon}}) = \sum_{ij} \int_0^{\dot{\varepsilon}_{ij}} \sigma_{ij}\, d\dot{\varepsilon}_{ij} \quad \text{or} \quad G(\dot{\bar{\varepsilon}}) = \int_0^{\dot{\bar{\varepsilon}}} \bar{\sigma} \cdot d\dot{\bar{\varepsilon}} \qquad [1]$$

$$J(\boldsymbol{\sigma}) = \sum_{ij} \int_0^{\sigma_{ij}} \dot{\varepsilon}_{ij}\, d\sigma_{ij} \quad \text{or} \quad J(\bar{\sigma}) = \int_0^{\bar{\sigma}} \dot{\bar{\varepsilon}} \cdot d\bar{\sigma} \qquad [2]$$

In these equations, $\dot{\varepsilon}_{ij}$ and σ_{ij} are the components of the strain rate and stress tensors, respectively, and $\dot{\bar{\varepsilon}}$ and $\bar{\sigma}$ denote the von Mises equivalent strain rate and stress.

These definitions were proposed (in a different notation) by Hill[9] in 1956 as applicable to viscoplastic materials by analogy with the equivalent functions $U(\boldsymbol{\varepsilon})$ and $V(\boldsymbol{\sigma})$ employed for elastic materials.[10] In the latter case, $U(\boldsymbol{\varepsilon})$ represents the *strain energy density*, as given by

$$U(\boldsymbol{\varepsilon}) = \sum_{ij} \int_0^{\varepsilon_{ij}} \sigma_{ij}\, d\varepsilon_{ij} \qquad [3]$$

from which it follows that

$$\sigma_{ij} = \frac{\partial U}{\partial \varepsilon_{ij}} \qquad [4]$$

It is of particular interest that $U(\boldsymbol{\varepsilon})$ coincides with the internal energy per unit volume stored in the material under load; this energy component is recoverable on unloading.

The so-called *complementary energy density* $V(\boldsymbol{\sigma})$ does not have such a straightforward physical interpretation. It is derivable from $U(\boldsymbol{\varepsilon})$ by means of the following Legendre dual transformation:

$$V(\boldsymbol{\sigma}) = \sum_{ij} \sigma_{ij}\, \varepsilon_{ij} - U \qquad [5]$$

As

$$V(\boldsymbol{\sigma}) = \sum_{ij} \int_0^{\sigma_{ij}} \varepsilon_{ij}\, d\sigma_{ij} \qquad [6]$$

it is evident that

$$\varepsilon_{ij} = \frac{\partial V}{\partial \sigma_{ij}} \qquad [7]$$

Furthermore, in the case of *linear* elastic materials, $U = V = \sum_{ij} \sigma_{ij}\varepsilon_{ij}/2$.

Figures 1(a) and (b) illustrate elastic and viscoplastic cases, where the stress, strain, and strain rate tensors can be reduced to single components (*e.g.*, as in uniaxial tension). In Figure 1(a), U and V are represented by the areas below and above the stress-strain curve, respectively. In a

F. MONTHEILLET, Director of Research, on leave from the Microstructures and Processing Laboratory, Ecole des Mines, URA CNRS 1884, Saint-Etienne, France, and J.J. JONAS, Professor, are with the Department of Metallurgical Engineering, McGill University, Montreal, PQ, Canada H3A 2A7. KENNETH W. NEALE, Professor, is with the Faculty of Applied Science, University of Sherbrooke, PQ, Canada J1K 2R1.

Discussion submitted January 26, 1995.